AJNR

High Fractional Anisotropy in Brain Abscesses versus Other Cystic Intracranial Lesions

Rakesh K. Gupta, Khader M. Hasan, Asht M. Mishra, Deepak Jha, Mazhar Husain, Kashi N. Prasad and Ponnada A. Narayana

AJNR Am J Neuroradiol 2005, 26 (5) 1107-1114
http://www.ajnr.org/content/26/5/1107

High Fractional Anisotropy in Brain Abscesses versus Other Cystic Intracranial Lesions

Rakesh K. Gupta, Khader M. Hasan, Asht M. Mishra, Deepak Jha, Mazhar Husain, Kashi N. Prasad, and Ponnada A. Narayana

BACKGROUND AND PURPOSE: **It is known that intracranial mass lesions are relatively isotropic on diffusion-weighted imaging. The purpose of this study is to report an unusually high fractional anisotropy (FA) and mean diffusivity (D_{av}) in the cavity of the brain abscess compared with other cystic lesions.**

METHODS: **We performed diffusion tensor imaging (DTI) in 12 patients with cystic intracranial lesions (pyogenic abscess, $n = 5$; cysticercus cysts, $n = 2$; and low-grade astrocytoma, $n = 5$). Mean FA, D_{av} from the lesion core, perifocal edema, and corresponding contralateral normal-appearing regions were measured and compared for relative changes in these parameters. In the abscess cases, we placed regions of interest on areas with FA >0.2 and FA <0.2 to get FA and D_{av} values.**

RESULTS: **There were two patterns of FA values in the abscess cavity in all five patients. Part of the abscess showed mean FA = 0.440 ± 0.135, with $D_{av} = (0.993 \pm 0.185) \times 10^{-3}$ mm^2/s, whereas other parts had FA = 0.131 ± 0.039 with $D_{av} = (0.824 \pm 0.183) \times 10^{-3}$ mm^2/s. The cystic tumors and neurocysticercosis showed very high $D_{av} = (2.806 \pm 0.25, 2.654 \pm 0.35) \times 10^{-3}$ mm^2/s, with low FA = (0.108 ± 0.037, 0.08 ± 0.01), respectively.**

CONCLUSION: **Brain abscess cavity shows regions of increased FA values with restricted mean diffusivity compared with other cystic intracranial lesions. This information may prevent misinterpretation of the DTI information as white matter fiber bundle abnormalities associated with mass lesions.**

Diffusion is anisotropic in white matter fiber tracts, as axonal membranes and myelin sheaths present barriers to the motion of water molecules, in directions not parallel to their own orientation (1). The direction of maximal diffusivity has been shown to coincide with the white matter tract information. This information is contained in the diffusion tensor, a mathematical construct of diffusion in 3D space (1, 2). Currently, information about fiber tracts obtained from diffusion tensor imaging (DTI) is being used by neurosurgeons in the planning of tumor resection (2).

A brain abscess is characteristically defined as a focal suppurative process within the brain parenchyma (3). It forms important differential diagnosis with other tumor and nontumor ring-enhancing brain lesions (3). MR imaging techniques such as proton MR spectroscopy and diffusion-weighted (DW) imaging have been used in the differentiation of abscesses from nonabscess lesions with considerable success (4–6). Although most abscesses show restricted diffusion, there are reports showing high diffusivity in the treated abscesses and restricted diffusion in cystic metastases (4, 7, 8). It is proposed that combining DW imaging with *in vivo* proton MR spectroscopy may help in better characterization of these lesions (6).

In this work, we report remarkably high fractional anisotropy (FA) from the cavity of brain abscess in five patients with restricted mean diffusivity in comparison to nonabscess cases. An attempt is made to explain this unusual observation, which, to the best of our knowledge, is described here for the first time in the literature.

Subjects and Methods

We performed MR imaging, including DTI, on 12 consecutive subjects with various intracranial mass lesions. There were seven male and five female subjects ranging in age from 4 to 55

Received July 26, 2004; accepted after revision October 6.

From the Departments of Radiodiagnosis (R.K.G., A.M.M.) and Microbiology (K.N.P.), Sanjay Gandhi Postgraduate Institute of Medical Sciences, and the Department of Neurosurgery (D.J., M.H.), King George's Medical University, Lucknow, India; and the Department of Radiology (K.M.H., P.A.N.), University of Texas Medical School at Houston, Houston, Texas.

Supported by a grant from Indian Council of Medical Research, New Delhi, India.

Address correspondence to Rakesh K. Gupta, MD, Department of Radiodiagnosis, Sanjay Gandhi Postgraduate Institute of Medical Sciences, Lucknow-226014, India.

years. Five patients had brain abscess, five had low-grade astrocytoma, and two had neurocysticercosis (NCC). In the two patients with NCC, there were a total of five cysts of >2 cm in diameter. The diagnosis in the abscess and tumor patients was based on aspiration and culture of the pus and histopathologic reports in cystic neoplasm, respectively. The source of primary infection was otitis media ($n = 2$), orbital infection ($n = 1$), and tooth infection ($n = 2$). The pus was evaluated for the number of viable leukocytes and microbial culture. The final diagnosis in patients with NCC was based on the demonstration of scolex on conventional imaging and CSF serology (enzyme-linked immunosorbent assay) positive for the parasitic antigen (9). Repeat imaging, including DTI, was also performed in three patients with abscess to look for the changes in FA following aspiration of the pus. We have also obtained DTI data from 10 healthy age- and sex-matched control subjects for the purpose of comparison with these subjects.

MR Imaging Protocol

Whole-brain conventional MR imaging and DTI were acquired on a 1.5-T MR imaging scanner (General Electric Medical System, Milwaukee, WI) using a standard quadrature birdcage receive and transmit radio-frequency head coil. The conventional MR imaging protocol included T2-weighted fast spin-echo (SE) images with repetition time TR/TE/NEX) = 6000/200/16/2 and SE images with TR/TE/NEX = 1000/14/1. Both T1- and T2-weighted images were acquired from axial sections of 5-mm section thickness with 0.5-mm intersection gap and 240-mm FOV. Postcontrast T1-weighted magnetization transfer (MT) MR imaging was done after injecting gadolinium diethylenetriaminepenta-acetic acid in the dose of 0.1 mmol/kg body weight (Schering, Berlin, Germany), using the same parameters as T1 except for the off-resonance pulse (1.2 kHz) with pulse duration of 16 milliseconds and 670° flip angle to improve the sensitivity of the enhancement.

DTI data were acquired using a single-shot echo-planar dual SE sequence with ramp sampling (10, 11). The dual SE sequence reduces image distortions in the diffusion-weighted images by compensating for the effect of eddy currents as shown elsewhere (12). The sequence used spectral-selective pulses for fat suppression. The diffusion-weighted sequence incorporated symmetric trapezoidal gradient pulses with pulse duration ($\delta \sim 25$) and separation ($\Delta \sim 28$ ms). The diffusion weighting b-factor was set to 1,000 s/mm^{-2}, TR ~ 8 seconds, and TE ~ 100 ms. A total of 20–34 axial sections were acquired with a section thickness of 3 mm, no gap, FOV = 240 mm x 240 mm, and an image matrix of 256 × 256 (following zero-filling). The diffusion tensor encoding used was the balanced (13), rotationally invariant (14, 15) icosahderal scheme with 21 uniformly distributed directions over the unit hemisphere. To enhance the signal intensity-to-noise ratio (SNR) and reduce phase fluctuations, the magnitude constructed images were repeated (NEX = 4) and temporally averaged by the scanner software (10). The SNR_0 in the (b ~ 0) image was about 50 (parenchyma), which reduces the SNR-related biases in the DTI estimated metrics (15, 16). Data from a spherical water phantom were also acquired at 19°C by using the same DTI scheme for the purpose of *b*-factor calibration.

DT-MR Imaging Data Analysis

The magnitude-averaged data were transferred via file transfer protocol to a workstation for further analysis. In general, the DTI data analysis involves three major steps: preprocessing, processing, and postprocessing.

Data Preprocessing

The collected raw images were cropped and stripped using a semiautomated procedure to remove the scalp for isolating the brain. The DW imaging data were spatially filtered with a 3 × 3 median window. The data were then distortion-corrected for shear, scale, rotation, and translation by using the DT-MR imaging toolbox, which calls the 2D perspective models in the automated image and registration package (17, 18).

Data Processing

The distortion-corrected data were then interpolated to attain isotropic voxels and decoded to obtain the tensor field for each voxel. The tensor-filed data were then diagonalized using the analytical diagonalization method (19) to obtain the eigenvalues (λ_1, λ_2, and λ_3) and the three orthonormal eigevectors (e_1, e_2, and e_3). The tensor field data and eigenvalues were then used to compute the DTI metrics such as the mean diffusivity (D_{av}; equation 1) and fractional anisotropy (20) (FA; equation 2) for each voxel.

$$1) \qquad D_{av} = \frac{\lambda_1 + \lambda_2 + \lambda_3}{3}$$

Data Postprocessing and Quantification

To facilitate region-of-interest placement for quantitative analysis, the DTI-derived maps were displayed and overlaid on images with different contrasts in the three orthogonal planes for a visual inspection. FA regional values were obtained by placing the regions of interest on the abscess cavity and other cystic lesions on all sections that contained the lesions. The region-of-interest placement on the lesions was based on the FA maps overlayed on the D_{av} with a cut-off value of 0.20 so that voxels could be separated between the ones with FA values >0.20 and <0.20 for all the cystic lesions. This threshold was chosen because white matter was found to have this as minimal of 0.2 FA value in hundreds of brain images that we had analyzed. In addition, the same regions of interest were placed on the perifocal edema and the corresponding contralateral normal-appearing parenchyma as depicted by T2-weighted images. Size of the regions of interest was guided by the lesion size, and it was always more than 3 × 3 pixels in all the cases and typically 8 × 8 pixels, with shape varying from elliptical to rectangular. Data processing and analysis were performed using the analysis and design DTI-toolbox implemented under interactive data language (IDL) (Research Systems, Boulder, CO). FA and D_{av} from the whole brain from three healthy subjects were also quantified for the purpose of comparison.

Results

Water Phantom Data

For the purpose of quality control and *b*-factor calibration of the scanner gradient system, quantitative FA and diffusivities data were obtained from 25,000 voxels at the center of the water phantom gave $\lambda_1 = (2.05 \pm 0.08) \times 10^{-3}$ mm^2/s, $\lambda_2 = (1.99 \pm 0.07) \times 10^{-3}$ mm^2/s, $\lambda_3 = (1.90 \pm 0.06) \times 10^{-3}$ mm^2/s, $D_{av} = (1.98 \pm 0.06) \times 10^{-3}$ mm^2/s, and FA = 0.04 ± 0.02. Our water phantom calibration results are consistent with published literature at comparable room temperature (21).

Clinical Data

The abscesses were located in the right caudate nucleus ($n = 2$), right temporal lobe ($n = 1$), right temporoparietal region ($n = 1$), and right frontal region ($n = 1$). These appeared hyperintense on T2-

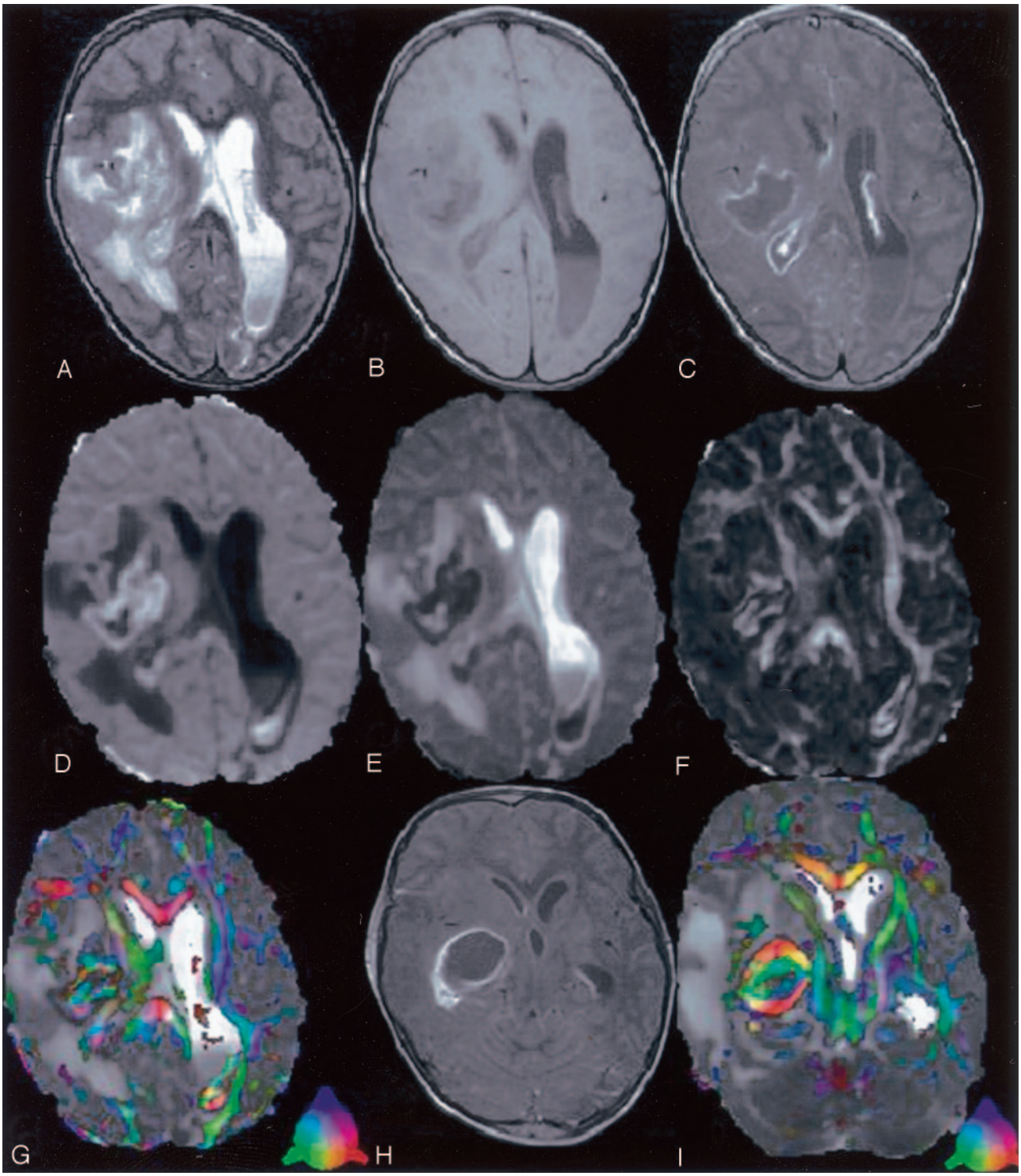

FIG 1. A 4-year-old child presented with right ear discharge and brain abscess with intraventricular rupture and meningitis.

T2-weighted axial image (*A*) through the lateral ventricles shows hyperintensity in the right periventricular region with mass effect. Note the layering in the left lateral ventricle. Corresponding T1-weighted image (*B*) shows the periventricular lesion as hypointense that displays rim enhancement on post contrast T1-weighted MT image (*C*). Note the enhancement of the ventricular lining that is more prominent on the right side, which suggests ependymitis (*C*). DW image (*D*) and D_{av} map (*E*) at the same level show restricted diffusion in the cavity. Note the area of restricted diffusivity in the layered portion of the left lateral ventricle. FA map (*F*) shows areas of high FA values in the cavity mixed with intervening low FA values. Note the high FA values in the lower part of the left lateral ventricle medial to the optic radiation. Color modulated FA maps fused with D_{av} map shows (*G*) orientation in the abscess cavity as well in the left lateral ventricle similar to what is observed in the oriented white matter. Three sections caudally, postcontrast T1-weighted MT image (*H*) shows the epicenter of the abscess cavity that appears highly oriented on the color-modulated FA maps fused with D_{av} images. The measured FA values were higher than corpus callusm in some of the regions of the abscess cavity. The color coding is shown (*G* and *I,* lower left corner): red (right–left), green (anteroposterior), blue (superior–inferior).

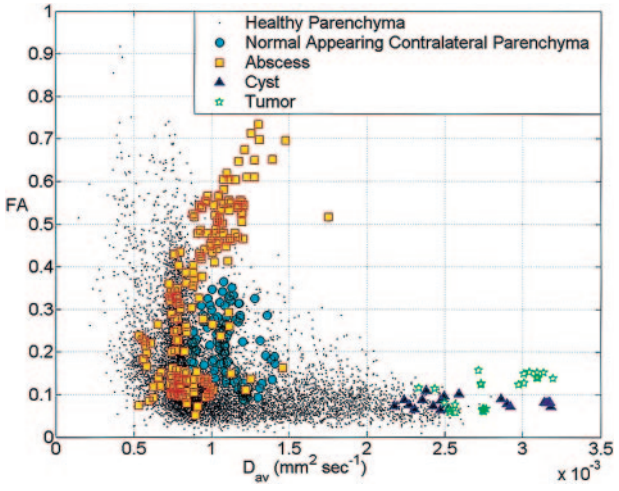

FIG 2. Scatter plot of the FA values versus D_{av} from the abscess cavities, tumor cavities cysts, corresponding contralateral normal-appearing parenchyma and whole brain of a healthy adult subject. The plot shows FA and D_{av} values for the tumor cavity and cyst are separate from the abscess cavity. Note the marked variability of FA values in the abscess cavity.

weighted images with peripheral hypointense rim, and iso- to hypointense on T1-weighted images. Postcontrast study showed rim enhancement. In one patient, the abscess ruptured into the right lateral ventricle with layering on T2, T1, and DW images and showed low D_{av} and high FA values in the layer (Fig 1). The culture from the pus grew *S. aureus* ($n = 2$), anaerobic streptococci ($n = 2$), and *Pseudomonas aeruginosa* ($n = 1$). The viable leukocyte count varied from 7,000 to 16,000 in all the abscess cases. The tumors were located in the cerebellum ($n = 2$), brain stem ($n = 1$), right parietal ($n = 1$), and left frontotemporal region ($n = 1$). These appeared hyperintense on T2 and hypointense on T1 and showed rim enhancement on postcontrast study. There was no viable cell visible on microscopy in the fluid obtained from the tumor cavity.

The axonal fibers around the cystic lesions showed displacement with marked decrease in FA values in the regions of edema when present focally. The changes in FA at different locations of the abscess, cystic tumors, NCC, and corresponding contralateral normal-appearing white matter and from the normal healthy individuals are plotted against D_{av} (Fig 2). Part of the abscess with FA >0.2 and <0.2 showed mean FA = 0.440 ± 0.135 with D_{av} = (0.993 ± 0.185) × 10^{-3} mm^2/s, and FA = 0.131 ± 0.039 with D_{av} = (0.8237 ± 0.183) × 10^{-3} mm^2/s, respectively (Figs 1–3). The cystic tumors (Fig 4) and NCC (Fig 5) showed very high D_{av} = (2.806 ± 0.25) × 10^{-3} mm^2/s, (2.654 ± 0.35) × 10^{-3} mm^2/s with low FA values ~ (0.108 ± 0.037 and 0.08 ± 0.01), respectively. The mean FA and D_{av} values from the perifocal edema normal-appearing corresponding contralateral parenchyma were 0.0751 ± 0.021, 0.208 ± 0.07, and (1.708 ± 0.27, 1.096 ± 0.13) × 10^{-3} mm^2/s, respectively. The D_{av} values were toward the higher side compared with the normal healthy subjects and the normal values reported in the literature (10). This is probably due to voxel contamination with CSF and the effect of pressure on the contralateral lobe by the pathology causing the increased water content in these regions. In three patients with brain abscess, a repeat study following surgical intervention showed a marked decrease in the residual cavity with no restriction of diffusion (Fig 3).

Discussion

The effect of cerebral neoplasm on the white matter tracts has been described using DTI as compressive, discontinued in the region of edema or tumor, or disrupted due to tumor infiltration (2, 22–24). This information was found to be useful for the purpose of tumor resection. We also observed displacement of the axons surrounding the lesions irrespective of the nature of the lesion along with low FA values in the region of the perifocal edema. In addition, in this study we observed markedly increased FA in the cavity of the abscess with different orientations that was not observed in the cavity of the cystic astrocytomas and neurocysticercosis (Figs 1–5).

The MR features of a brain abscess vary with the lesion stage. During the initial cerebritis stage, an ill-defined subcortical hyperintense zone on T2-weighted images is associated with poorly delineated enhancing areas within the iso- to mildly hypointense edematous region on enhanced T1-weighted images. During the early and late capsule stages, the collagenous abscess capsule is visible on precontrast study as a comparatively thin-walled, well-delineated iso- to slightly hyperintense rim that becomes hypointense on T2-weighted sequences (3). These abscesses usually show restricted diffusion on DW imaging with low mean diffusivity (3, 5, 6). The purulent material obtained from the abscess cavity at the time of surgery shows inflammatory cells, necrotic cellular debris, proteins, and amino acids as well as low molecular weight metabolites (3, 25). In the present study, in addition to low diffusivity, we observed high FA in some part of the abscess cavity with orientation on the principal eigenvector maps in all of these cases. The FA values are as high as the normal white matter with orientation apparently suggesting an oriented structure within the cavity. Histologically, there was no structure other than the inflammatory cells, necrotic debris, proteins, and amino acids (3, 25). The high FA with low mean diffusivity has been described by several authors in cerebral ischemia and infarction. The previously reported FA values, however, were not as elevated as those observed in the current study (26–29). Recently, it has been shown that FA has a significant inverse correlation with T2 signal intensity in hyperacute stroke and there was no relation with D_{av} measures (29). It was proposed that the initial decrease in extracellular water resulted in high FA and low D_{av} (29). Increased FA has also been found in the first 24 hours after trauma with increased T2 and no change in D_{av} (30). This has been explained by an increase in the largest (λ_1) eigenvalue coupled with a

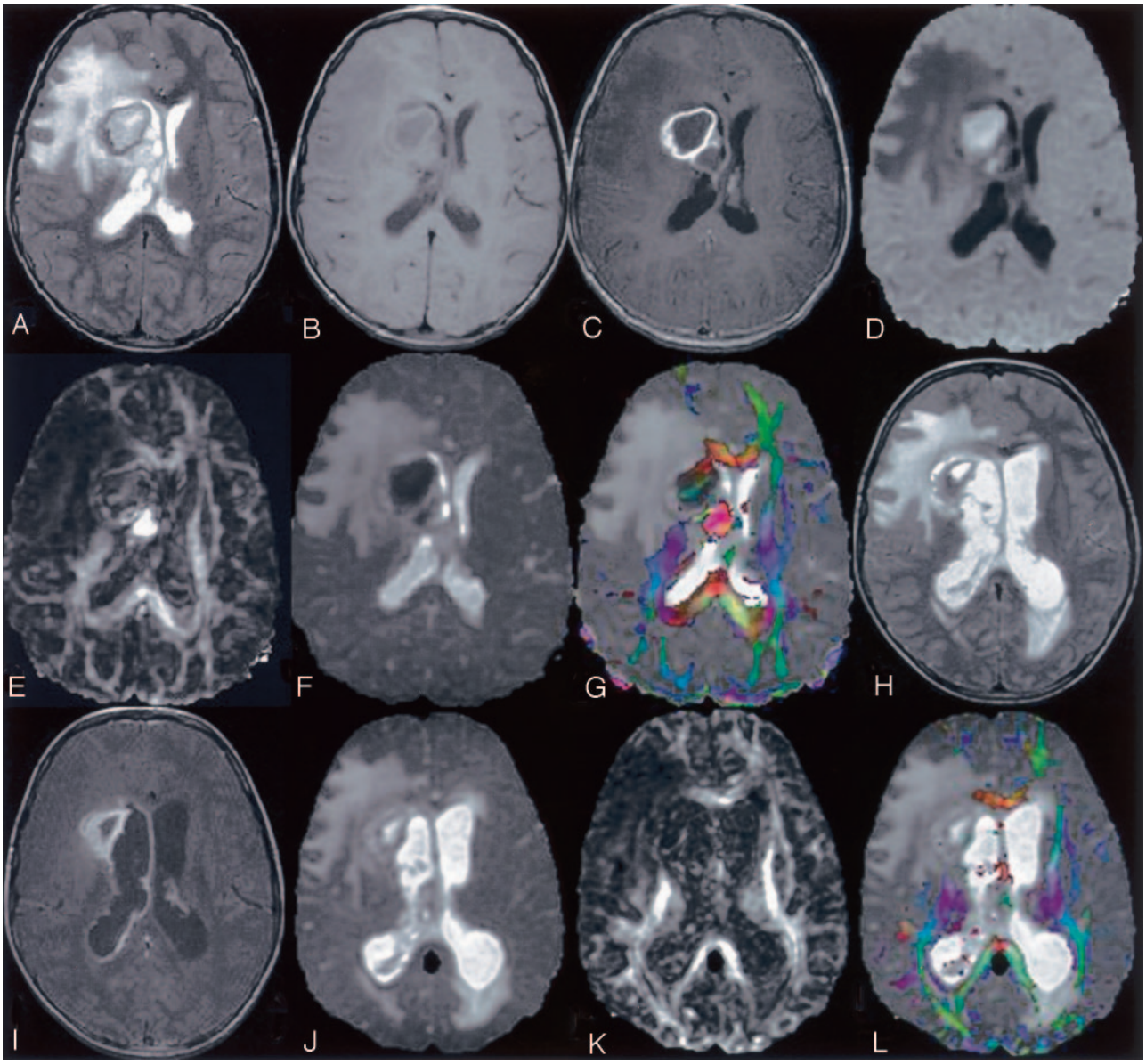

FIG 3. An 8-year-old girl presented with fever, tooth infection, and signs of raised intracranial tension.

T2-weighted axial image (*A*) through the lateral ventricles shows hyperintense lesion with hypointense peripheral rim in the right periventriclular region and is associated with mass effect. Corresponding T1 (*B*) and postcontrast T1-weighted MT (*C*) images show central hypointensity with peripheral rim extending to the body of the corpus callosum. DW image (*D*) and D_{av} map (*E*) show areas of restricted diffusivity. FA map (*F*) show very high values in the medial part of the abscess cavity, and variable FA in the lateral part of the cavity (0.12–0.32). Color-modulated FA map fused on D_{av} map shows (*G*) the same with orientation. Following drill aspiration of the abscess cavity, a repeat DTI was done after 5 days. Follow-up T2-weighted image (*H*) shows residual cavity with mild ventricular dilatation. Postcontrast T1-weighted MT image (*I*) shows rim enhancement of the residual cavity with ependymal enhancement, which suggests ependimitis. D_{av} map (*J*) shows high diffusivity and FA map (*K*) shows marked decrease in values compared with panel *F.* Color-modulated FA maps (*L*) fused with D_{av} shows the loss of orientation compared with panel *G.*

proportionately smaller decrease in the smallest (λ_3) eigenvalue (30). The present clinical situation, however, is not similar to hyperacute stroke or acute traumatic brain injury and therefore cannot be explained on this basis. We propose that the inflammatory cells in the abscess cavity become oriented and organized, resulting in high diffusion anisotropy. The current observation, however, challenges the traditional view that brain anisotropy usually represents myelination and axonal packing (1, 2, 10, 11, 23, 24) and calls for some caution in the interpretation of DTI data.

A number of studies have reported DTI results in brain tumors. The tumors have been shown to displace white matter tracts due to mass effect. In all published studies, there is an isotropic diffusion at the center of the cystic tumor cavity (3, 22, 24). We have observed 0–5 intact cells/mm^3 in the fluid obtained from 45 cystic brain neoplasms and three cysticercus cysts (authors' unpublished data). On the other hand,

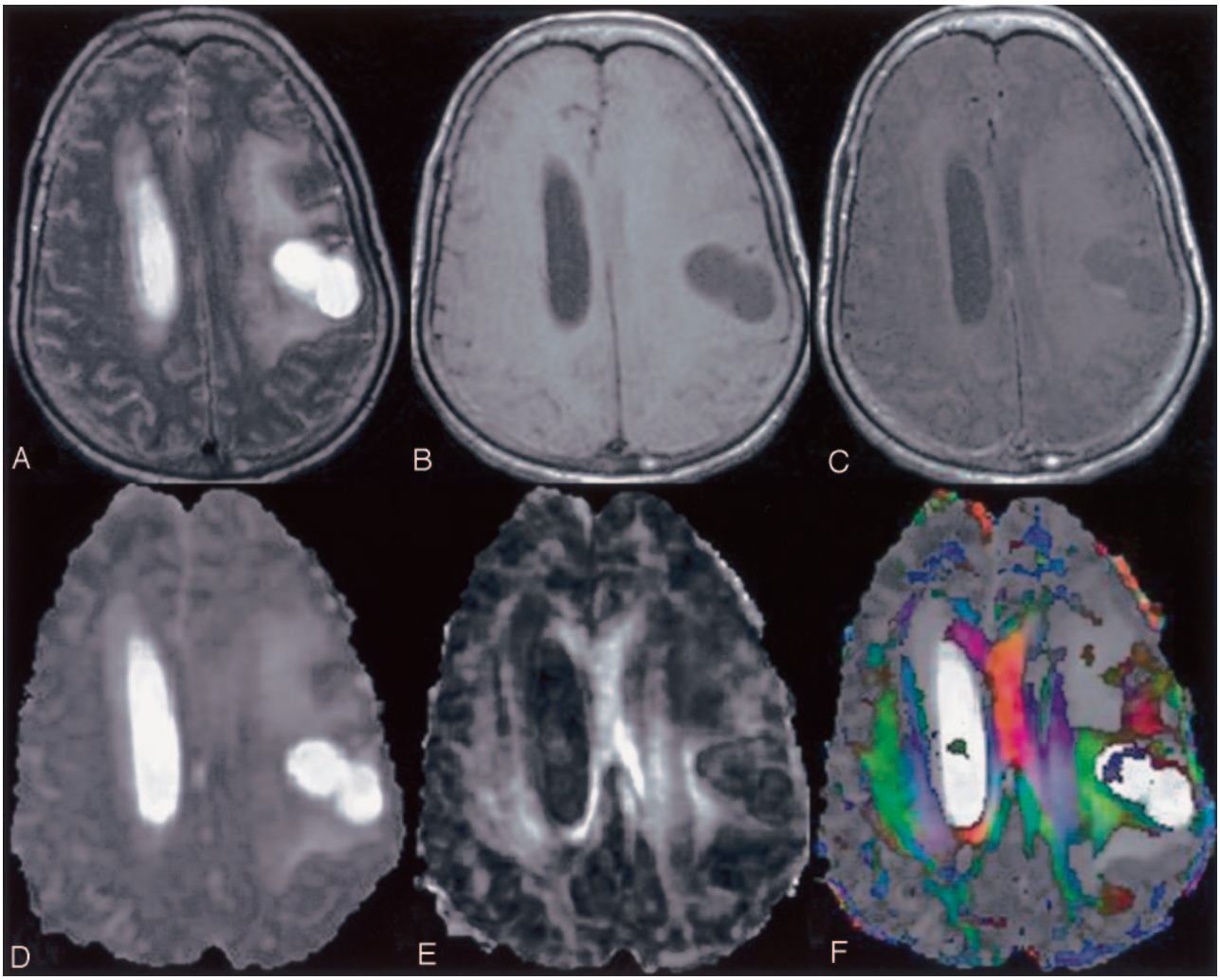

FIG 4. A 55-year-old woman with left frontoparietal low-grade astrocytoma.

T2-weighted axial image (*A*) through the lateral ventricle shows hyperintense mass on the left side with perifocal edema and mass effect. The lesion appears hypointense on T1WI image (*B*) and shows rim enhancement on postcontrast T1-weighted MT image (*C*). D_{av} map (*D*) shows high diffusivity and FA map (*E*) shows little anisotropy. Color-modulated FA map shows no orientation in the cavity.

a large number of intact inflammatory cells were seen in these patients with brain abscess. One possibility could be that these cells are tightly packed, thus reducing the extracellular space and therefore are responsible for a large anisotropy in the abscess cavity; however, this explanation is less likely. This is because we observed regions in the abscess cavity with high FA and restricted diffusion and another with low FA and restricted diffusion (Figs 1–3). Larger variation in FA values without a great difference in D_{av} of the abscess cavity suggests that FA does not have a strong relationship with D_{av} in the abscess model (Fig 2).

The host response to the microorganisms consists of three pathologic mechanisms: tissue inflammation, granuloma, and abscess formation (31). The presence of bacteria challenges the expression of leukocytes that are activated by its presence. This results in a release of large amounts of chemotactic peptides and an up-regulation of intracellular adhesion molecules (ICAM-1) that are recruited to the cell surface to mediate their aggregation via lymphocyte function-associated molecule 1 (LFA-1) (31–33). A large cellular aggregation has been shown by incubating the bacteria with the leukocytes after 5 hours that firm up after 24 hours (32). The capsular stage of the brain abscess occurs from the 10th day onward and is associated with the formation of a well-vascularized wall that sequesters the lesion. The cavity of the lesion contains inflammatory cells, bacteria, and debris (3). In the present study, viable leukocytes were found in the cavity and have grown microorganisms responsible for the abscess formation on pus culture. We postulate that the regions with high FA values in the cavity of the abscess contain aggregated (clumped) leukocytes due to the presence of adhesive molecules that are known to be up-regulated in the presence of bacteria. Low FA in some regions of the abscess cavity probably reflects areas devoid of leukocytes with adhesive properties due to the relative lack of up-regulation of the adhesive molecules on the sur-

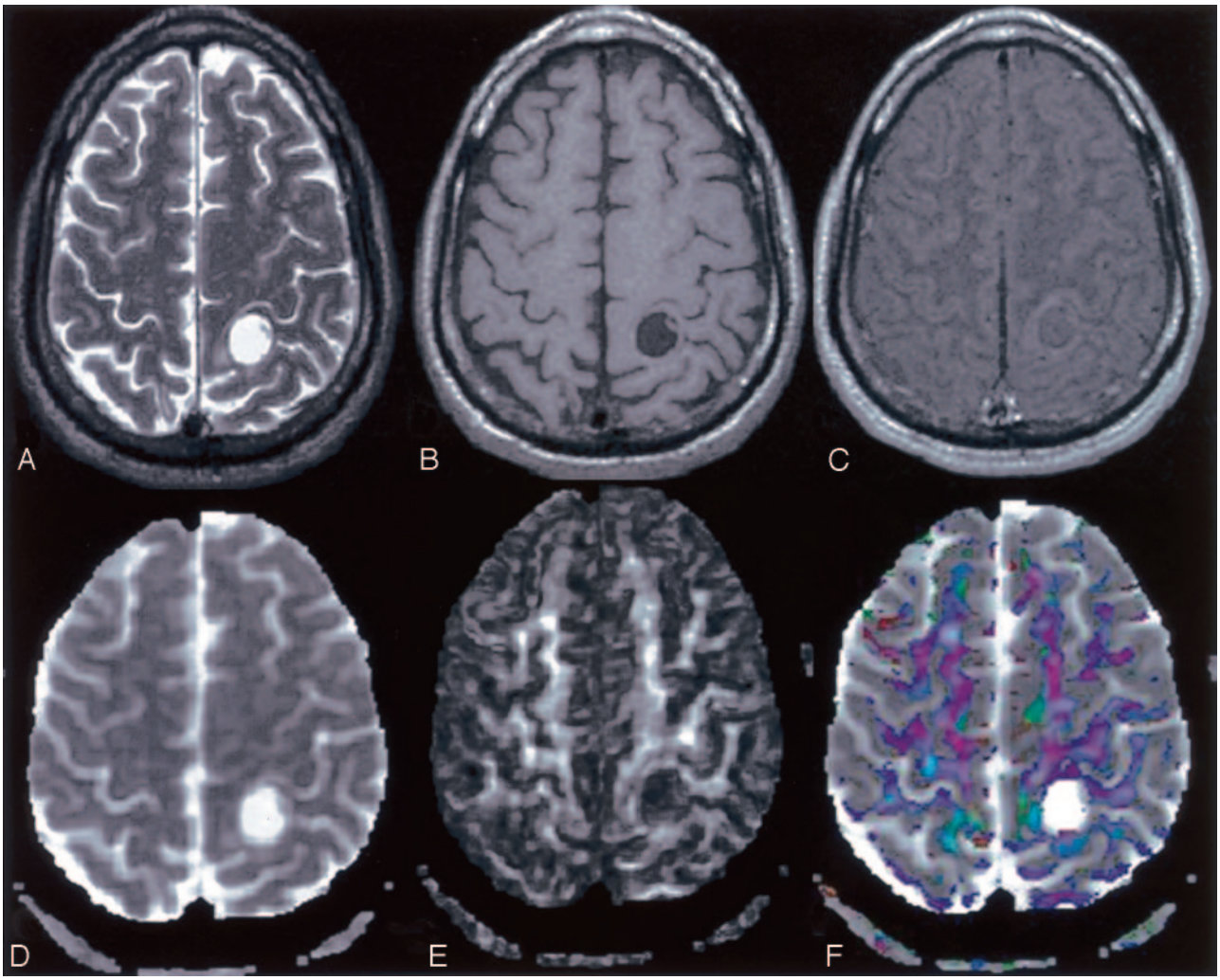

FIG 5. A 40-year-old man with neurocysticercosis.

T2-weighted image (*A*) through the supraventricular region shows a hyperintense cyst on the left side with eccentrically placed hypointense scolex. The lesion appears hypointense with isointense scolex on T1-weighted image (*B*), and shows minimal rim enhancement on postcontrast T1-weighted MT image (*C*). D_{av} map (*D*) shows high diffusivity, and FA map (*E*) shows little anisotropy. Color-modulated FA map shows no orientation in the cavity.

face of the remaining leukocytes. This hypothesis, however, needs confirmation by performing further studies to demonstrate the adhesive molecules on the surface of the leukocytes with cell clumping.

Conclusion

The present study demonstrates that brain abscess cavity shows regions of increased FA values with restricted mean diffusivity compared with other cystic intracranial lesions. With an increasing use of DTI in surgical planning of brain-tumor resection, one may become more careful in interpreting these changes as oriented axonal fibers.

References

1. Le Bihan D. **Looking into the functional architecture of the brain with diffusion MRI.** *Nat Rev Neurosci* 2003;4:469–480
2. Jellison BA, Field AS, Medow J, et al. **Diffusion tensor imaging of cerebral white matter: a pictorial review of physics, fiber tract anatomy, and tumor imaging patterns.** *AJNR Am J Neuroradiol* 2004;25:356–369
3. Venkatesh SK, Gupta RK. **Pyogenic infections.** In: Gupta RK, Lufkin RB, eds. *MR imaging and spectroscopy of central nervous system infection.* New York: Kluwer/Plenum;2001:57–93
4. Shukla-Dave A, Gupta RK, Roy R, et al. **Prospective evaluation of in vivo proton MR spectroscopy in differentiation of similar appearing intracranial cystic lesions.** *Magn Reson Imaging* 2001;19:103–110
5. Desprechins B, Stadnik T, Koerts G, et al. **Use of diffusion weighted MR imaging in differential diagnosis between intracerebral necrotic tumors and cerebral abscesses.** *AJNR Am J Neuroradiol* 1999;20:1252–1257
6. Mishra AM, Gupta RK, Jaggi RS, et al. **Role of diffusion-weighted imaging and in vivo proton magnetic resonance spectroscopy in the differential diagnosis of ring-enhancing intracranial cystic mass lesions.** *J Comput Assist Tomogr* 2004;28:540–547
7. Holtas S, Geijer B, Stromblad LG, et al. **A ring-enhancing metastasis with central high signal on diffusion-weighted imaging and low apparent diffusion coefficients.** *Neuroradiology* 2000;42:824–827
8. Mikami T, Saito K, Kato T, et al. **Detection and characterization of the evolution of cerebral abscesses with diffusion-weighted magnetic resonance imaging-two case reports.** *Neurol Med Chir (Tokyo)* 2002;42:86–90
9. Del Brutto OH, Rajshekhar V, White AC, et al. **Proposed diagnostic criteria for neurocysticercosis.** *Neurology* 2001;57:177–183

10. Le Bihan D. *Diffusion and perfusion magnetic resonance imaging: applications to functional MRI.* New York: Raven Press;1995:1–374
11. Basser PJ. **Inferring microstructural features and the physiological state of tissues from diffusion-weighted images.** *NMR Biomed* 1995;8:333–344
12. Reese TG, Heid O, Weisskoff RM, Wedeen VJ. **Reduction of eddy-current-induced distortion in diffusion MRI using a twice-refocused spin echo.** *Magn Reson Med* 2003;49:177–182
13. Hasan KM, Parker DL, Alexander AL. **Comparison of gradient encoding schemes for diffusion-tensor MRI.** *J Magn Reson Imaging* 2001;13:769–780
14. Batchelor PG, Atkinson D, Hill DL, et al. **Anisotropic noise propagation in diffusion tensor MRI sampling schemes.** *Magn Reson Med* 2003;49:1143–1151
15. Hasan KM, Narayana PA. **Computation of the fractional anisotropy and mean diffusivity maps without tensor decoding and diagonalization: theoretical analysis and validation.** *Magn Reson Med* 2003;50:589–598
16. Pierpaoli C, Basser PJ. **Toward a quantitative assessment of diffusion anisotropy.** *Magn Reson Med* 1996;36:893–906
17. Woods RP, Grafton ST, Holmes CJ, et al. **Automated image registration. I. General methods and intrasubject, intramodality validation.** *J Comput Assist Tomogr* 1998;22:139–152
18. Hasan KM, Alexander AL, Narayana PA. **Does fractional anisotropy have better noise immunity characteristics than relative anisotropy in diffusion tensor MRI? An analytical approach.** *Magn Reson Med* 2004;51:413–417
19. Hasan KM, Basser PJ, Parker DL, Alexander AL. **Analytical computation of the eigenvalues and eigenvectors in DT-MRI.** *J Magn Reson* 2001;152:41–47
20. Basser PJ, Pierpaoli C. **Microstructural and physiological features of tissues elucidated by quantitative-diffusion-tensor MRI.** *J Magn Reson B* 1996;111:209–219
21. Mills R. **Self-diffusion in normal and heavy water in the range 1–45.** *J Phys Chem* 1973;77:685–688
22. Witwer BP, Moftakhar R, Hasan KM, et al. **Diffusion-tensor imaging of white matter tracts in patients with cerebral neoplasm.** *J Neurosurg* 2002;97:568–575
23. Clark CC, Barrick TR, Murphy MM, Bell BA. **White matter fiber tracking in patients with space-occupying lesions of the brain: a new technique for neurosurgical planning?** *Neuroimage* 2003;20:1601–1608
24. Mori S, Frederiksen K, van Zijl PCM, et al. **Brain white matter anatomy of tumor patients evaluated with diffusion tensor imaging.** *Ann Neurol* 2002;51:377–380
25. Garg M, Gupta RK, Husain M, et al. **Brain abscesses: etiologic categorization with in vivo proton MR spectroscopy.** *Radiology* 2004;230:519–527
26. van der Toon A, Sykova E, Dijkhuizen RM, et al. **Dynamic changes in water ADC, energy metabolism, extracellular space volume, and tortuosity in neonatal rat brain during global ischemia.** *Magn Reson Med* 1996;36:39–44
27. Sorensen AG, Wu O, Copen WA, et al. **Human acute cerebral ischemia: detection of changes in water diffusion anisotropy by using MR imaging.** *Radiology* 1999;212:785–792
28. Green HA, Pena A, Price CJ, et al. **Increased anisotropy in acute stroke: a possible explanation.** *Stroke* 2002;33:1517–1521
29. Ozsunar Y, Grant PE, Huisman TAG, et al. **Evolution of water diffusion and anisotropy in hyperacute stroke: significant correlation between fractional anisotropy and T2.** *AJNR Am J Neuroradiol* 2004;25:699–705
30. Field AS, Hasan K, Jellison BJ, et al. **Diffusion tensor imaging in an infant with traumatic brain swelling.** *AJNR Am J Neuroradiol* 2003;24:1461–1464
31. Gibson FC 3rd, Onderdonk AB, Kasper DL, Tzianabos AO. **Cellular mechanism of intraabdominal abscess formation by Bacteroides fragilis.** *J Immunol* 1998;160:5000–5006
32. Moese S, Selbach M, Meyer TF, Backert S. **cag+ Helicobacter pylori induces homotypic aggregation of macrophage-like cells by up-regulation and recruitment of intracellular adhesion molecule 1 to the cell surface.** *Infect Immun* 2002;70:4687–4691
33. Kielian T, Hickey WF. **Proinflammatory cytokine, chemokine, and cellular adhesion molecule expression during the acute phase of experimental brain abscess development.** *Am J Pathol* 2000;157:647–658